NEOPLASIA
www.neoplasia.com

Volume 10 Number 8 August 2008 pp. 782–796 782

Progressive Metaplastic and Dysplastic Changes in Mouse Pancreas Induced by Cyclooxygenase-2 Overexpression[1]

Jennifer K.L. Colby*, Russell D. Klein†,2, Mark J. McArthur†, Claudio J. Conti*, Kaoru Kiguchi*, Toru Kawamoto*, Penny K. Riggs*,§, Amy I. Pavone*, Janet Sawicki¶ and Susan M. Fischer*

*University of Texas M.D. Anderson Cancer Center, Science Park – Research Division, Smithville, TX 78957, USA; †Department of Human Nutrition, Cancer Chemoprevention Program, The Ohio State University, Columbus, OH 43210, USA; ‡Michale E. Keeling Center for Comparative Medicine and Research, Department of Veterinary Sciences, University of Texas M.D. Anderson Cancer Center, Bastrop, TX 78602, USA; §Department of Animal Science, Texas A&M University, College Station, TX, 77843-2471, USA; ¶The Lankenau Institute for Medical Research, Wynnewood, PA, 19016, USA

Abstract

Cyclooxygenase-2 (COX-2) overexpression is an established factor linking chronic inflammation with metaplastic and neoplastic change in various tissues. We generated transgenic mice (BK5.COX-2) in which elevation of COX-2 and its effectors trigger a metaplasia–dysplasia sequence in exocrine pancreas. Histologic evaluation revealed a chronic pancreatitis-like state characterized by acinar-to-ductal metaplasia and a well-vascularized fibroinflammatory stroma that develops by 3 months. By 6 to 8 months, strongly dysplastic features suggestive of pancreatic ductal adenocarcinoma emerge in the metaplastic ducts. Increased proliferation, cellular atypia, and loss of normal cell/tissue organization are typical features in transgenic pancreata. Alterations in biomarkers associated with human inflammatory and neoplastic pancreatic disease were detected using immunohistochemistry. The abnormal pancreatic phenotype can be completely prevented by maintaining mice on a diet containing celecoxib, a well-characterized COX-2 inhibitor. Despite the high degree of atypia, only limited evidence of invasion to adjacent tissues was observed, with no evidence of distant metastases. However, cell lines derived from spontaneous lesions are aggressively tumorigenic when injected into syngeneic or nude mice. The progressive nature of the metaplastic/dysplastic changes observed in this model make it a valuable tool for examining the transition from chronic inflammation to neoplasia.

Neoplasia (2008) 10, 782–796

Abbreviations: BK5, bovine keratin 5; CFP, cyan fluorescent protein; COX, cyclooxygenase; CP, chronic pancreatitis; EP, PGE_2 receptor; H&E, hematoxylin and eosin; IHC, immunohistochemistry; K19, keratin 19; (m)PanIN, (mouse) pancreatic intraepithelial neoplasia; PaSC, pancreatic stellate cell; PDAC, pancreatic ductal adenocarcinoma; PGE_2, prostaglandin E_2

Address all correspondence to: Susan M. Fischer, The University of Texas M.D. Anderson Cancer Center, Science Park – Research Division, P.O. Box 389, 1808 Park Rd 1C, Smithville, TX 78957. E-mail: smfischer@mdanderson.org

[1]This work was supported by National Institutes of Health grants CA105345 and CA122815 (to S.M.F.) and a National Institute of Environmental Health Sciences (NIEHS) training grant T32 ES07247; and by a National Cancer Institute training grant R25CA57730 (J.K.L.C.) and ES07784 from NIEHS.

[2]In memoriam of Dr. Russell D. Klein (1962–2006): Russell D. Klein died December 1, 2006 after a long battle with leukemia. He was a promising young scientist, an exemplary mentor, and a fine human being. His presence will be greatly missed.

Received 26 February 2008; Revised 25 April 2008; Accepted 28 April 2008

Copyright © 2008 Neoplasia Press, Inc. All rights reserved 1522-8002/08/$25.00
DOI 10.1593/neo.08330

Introduction

Inflammatory conditions of the pancreas predispose individuals to developing pancreatic ductal adenocarcinoma (PDAC), exemplified by individuals with heritable or sporadic forms of chronic pancreatitis (CP) [1–3]. Among the general population, a number of risk factors for pancreatitis and pancreatic cancer have been identified, e.g., alcohol and tobacco use [4,5], high consumption of nitrosamines [6], and diabetes [7,8], which can lead to chronic inflammatory changes either in specific target tissues [5] or in the body as a whole [7,8]. Although many forms of CP have been linked to a higher risk for PDAC, the relationship between the two is ill-defined [9].

Metaplasia, the replacement of one mature cell type by another, frequently occurs in chronic inflammation, and is often considered a preneoplastic condition (e.g., Barrett metaplasia of the esophagus) [10]. Acinar-to-ductal metaplastic changes in the pancreas are often found in CP and in association with the recently defined pancreatic intraepithelial neoplasias (PanINs) and mouse PanIN (mPanIN) precursor lesions and PDAC [11–15]. Recent articles have attempted to clarify the relationship between CP and PDAC [12,14], and one study has demonstrated that acinar cells clearly contribute to the development of PanIN lesions [13]. Metaplastic ductal cells seem to have diminished sensitivity to apoptotic stimuli and, therefore, have a selective advantage in the diseased pancreas [16]. Although a great deal of evidence exists supporting high-grade PanINs as precursor lesions of PDAC, and this is widely accepted, questions remain with regard to the validity of ductal complexes as precursors to PDAC [17]. The concept is supported by evidence from groups studying both rodent and human forms of the disease [18–21].

Cyclooxygenases (COX-1 and -2) are rate-limiting enzymes in the production of prostaglandins (PGs), which are short-lived lipid-signaling molecules involved in a number of biologic functions [22]. COX-1 expression is generally constitutive, whereas COX-2 is usually induced by stimuli involved in inflammatory responses. Prostaglandin E_2 (PGE_2), a primary metabolite of COX-2, has been shown to promote cell survival, proliferation, and angiogenesis and prohibit apoptosis, all processes influencing cancer development [23].

Prostaglandin production is frequently a factor in the development and maintenance of chronic inflammation, and COX-2 is upregulated in numerous human cancers and precancerous conditions, including pancreatitis and PDAC [24,25]. Cyclooxygenase-2 expression has also been found to be an early event in the *N*-nitrosobis-(2-oxo-propyl)amine model of pancreatic carcinogenesis in hamster [26]. Forced COX-2 overexpression is associated with the development of cancer in mouse models of mammary [27] and bladder [28] tumorigenesis. In the skin of NMRI mice, COX-2 overexpression driven by the bovine keratin 5 (BK5) promoter does not lead to spontaneous tumor development but sensitizes the skin to chemical carcinogenesis [29]. In this same model, high PGE_2 levels also lead to fibrocystic changes and epithelial lesions in the mammary gland and, to some extent, in the pancreas [30,31].

In this article, we present a mouse model, FVB-*Tg(KRT5-Ptgs2)7Sf* mice, hereafter referred to as BK5.COX-2 mice, in which the overexpression of COX-2 under the control of a BK5 promoter drives pancreatic acinar-to-ductal metaplasia progressing to severe dysplasia suggestive of PDAC. Histopathologic analyses reveal similarities to human CP, as well as pancreatic lesions observed in other genetically [32,33] or chemically induced [34,35] animal models of pancreatic disease. BK5.COX-2 pancreatic lesions are characterized by acinar-to-ductal metaplasia, development of a fibroinflammatory stroma, increased proliferation of metaplastic ductal cells, nuclear pleomorphism, and abnormal cell and tissue architecture. Pancreata frequently develop multilocular cysts. The BK5.COX-2 pancreatic phenotype is initiated and primarily driven by high levels of COX-2 activity/PGE_2 signaling. The malignant potential of spontaneous BK5.COX-2 lesions to progress to invasive adenocarcinoma is suggested by the presence of strongly dysplastic cell/tissue morphology and by the establishment of cell lines that form aggressive tumors when injected to either syngeneic or nude mice. We propose that these mice represent a valuable new model for the assessment of chemopreventive and chemotherapeutic agents in pancreatic disease, particularly those associated with pronounced inflammatory conditions such as CP.

Materials and Methods

Mice

All housing and procedures were carried out in an animal facility accredited by the American Association for the Assessment and Accreditation of Laboratory Animal Care, in accordance with Institutional Animal Care and Use Committee guidelines. Mice were maintained on chow *ad libitum*, unless specified otherwise. FVB-*Tg(KRT5-Ptgs2)7Sf* (BK5.COX-2) mice were generated on the FVB background by pronuclear injection of a bovine keratin 5 (BK5) promoter construct containing the coding region of the mouse COX-2 gene, the rabbit β-globin intron, and an SV40 poly-A tail. The BK5 promoter directs expression to several tissue types, namely, basal cells of skin, prostate, bladder, forestomach, mammary myoepithelium, kidney papilla, and pancreatic ductal epithelia [36]. Transgenic mice can consistently be identified by a sparse hair coat but showed no other visible abnormalities.

Two founders (Lines 7 and 9) were generated, both of which had a pancreatic phenotype. Founder 9 produced no offspring; for all subsequent studies, we used mice from Line 7. To maintain the line, BK5.COX-2 males were bred to wild type female FVB mice. Hemizygous offspring were used for all subsequent analyses. Prostaglandin production due to higher COX-2 expression in transgenic embryos was sufficient to trigger premature parturition; to avoid this, dams were fed low levels of indomethacin (4 ppm of AIN-76A diet; Research Diets, St. Paul, MN) for the last few days of pregnancy. Litters born to these females were full term and otherwise healthy; we noticed no long-term effects attributable to indomethacin treatment.

COX-2 Genotyping Polymerase Chain Reaction

Primers used recognize the rabbit β-globin intron within the transgene; sequences are as follows: 5′-TCA-AAG-ACA-CTC-AGG-TAG-AG-3′ (forward); 5′-CTT-GAG-TTT-GAA-GTG-GTA-AC-3′ (reverse). For a single 50-μl reaction, the following amounts were added: 37.8 μl of double-distilled H_2O, 5 μl of 10× polymerase chain reaction (PCR) buffer, 1.0 μl of 10 mM dNTPs, 0.5 μl each of forward and reverse primers, 0.2 μl of *Taq* polymerase, and 5 μl sample from HotShot DNA extraction. DNA was amplified using the following PCR conditions: an initial denaturation at 95°C (1 minute), 30 cycles of denaturation, annealing, and extension at 95°C (30 seconds), 50°C (30 seconds), and 72°C (30 seconds), respectively, and a final extension at 72°C (5 minutes), followed by a 4°C hold.

Histologic Evaluation and Immunohistochemistry

Tissues were embedded in paraffin blocks, and 4-μm sections were cut. Slides were deparaffinized in a xylene substitute (CitraSolv; LLC,

Danbury, CT) for 2 × 5 minutes. Tissues were hydrated in a series of alcohols and water before undergoing antigen retrieval. The antigen retrieval method used was dependent on the specific antibody. Methods used include microwaving in 10-mM citrate buffer, protease treatment, and EDTA treatment. After antigen retrieval, endogenous peroxidase activity was quenched with hydrogen peroxide (3% for 10 minutes), and sections were blocked with 10% normal serum in phosphate-buffered saline (PBS) for 30 minutes. Primary antibodies were applied in the concentrations for the lengths of time stated in Table 1 (detailed antibody protocols are available on request). Slides were washed two times for 5 minutes in PBS before application of the secondary antibody. For most antibodies, slides were incubated with the secondary antibodies for 30 minutes, and again washed several times with PBS. Staining was developed by incubating sections with diaminobenzidine; sections were counterstained with hematoxylin. Slides were dehydrated in a series of alcohols before coverslipping.

Special Stains

Tissue sections were prepared as previously mentioned for hematoxylin and eosin (H&E). Toluidine blue: slides were stained with a 0.1% solution of toluidine blue for 5 minutes and were briefly destained before dehydration and coverslipping. Alcian blue and periodic acid Schiff (PAS): slides were stained using kits (KTABP2.5 for Alcian blue and KTPAS for PAS) from American Master-Tech Scientific, Inc. (Lodi, CA).

BK5.CFP Mice/Detection of Cyan Fluorescent Protein

To construct pK5.CFP, the plasmid pECFP (Clontech, Mountain View, CA) was digested with *Bam*HI and *Afl*II. A 1-kb fragment containing the CFP sequence was ligated to (*Bam*HI + *Afl*II)–digested pIND (Stratagene, La Jolla, CA) to create pIND.ECFP. pIND.ECFP was digested with *Bam*HI and *Nhe*I. The 1-kb fragment was ligated to (*Bgl*II + *Nhe*I)–digested pMECA [37] to create pMECA-ECFP. A 7-kb fragment, released by *Kpn*I digestion of the plasmid p3/4 (gift from Deutsches Krebsforchungzentrum, Heidelberg, Germany), was digested with *Sal*I. The resulting 5.2-kb fragment containing the BK5 promoter sequence was ligated to (*Kpn*I + *Xho*I)–digested pMECA-ECFP to create pK5.CFP. pK5.CFP was digested with *Nhe*I and *Kpn*I, and the resulting 6.2-kb transgene fragment, containing the keratin 5 promoter and the cyan fluorescent protein (CFP), was purified and microinjected into fertilized B6C3F1 mouse oocytes as described [38]. To observe CFP fluorescence in the pancreas of transgenic mice, pancreata were fixed in 4% paraformaldehyde for 30 minutes at room temperature, washed three times in PBS, and mounted in OCT for frozen sectioning. Frozen sections were observed using a fluorescent microscope (Axioplan; Zeiss, Jena, Germany) equipped with a CFP filter set and an Axioplan camera.

RNA Extraction

We used the following protocol to avoid degradation due to the high levels of RNAses present in pancreas. The protocol is based on

Table 1. List of Antibodies and Conditions Used.

Primary Antibody	Application	Source	Dilution	Incubation Time/Temperature	Antigen Retrieval Method
α-SMA	IHC	Dako	1:1000	30 minutes, RT	None
Amylase	IHC	Sigma	1:5000	30 minutes, RT	Citrate*
β-Catenin	IHC	BD Biosciences	1:500	30 minutes, RT	Citrate
Caspase 3 (active)	IHC	R&D Systems	1:2000	30 minutes, RT	Citrate
CD3	IHC	Serotec	1:100	2 hours, RT	EDTA†
CD31¶	IHC	Pharmingen	1:400	ON, 4°C	Protease‡
CD45R	IHC	Serotec	1:2000	1 hour, RT	Citrate
COX-1	WB	Cayman	1:100	ON, 4°C	N/A
COX-2	IHC	Cayman	1:500	1 hour, RT	Citrate
E-Cadherin	IHC	Santa Cruz Biotechnology	1:50	1 hour, RT	Citrate
Insulin	IHC	Zymed	1:500	1 hour, RT	None
K19	IHC	AbCam	1:100	1 hour, RT	EIER§ (pepsin)
Ki-67	IHC	Dako	1:200	ON, 4°C	Citrate
MMP-9	WB	Chemicon	1:1000	1 hour, RT	N/A
MMP-7	IHC	LabVision/Neomarkers	1:50	1 hour, RT	None
Pan-S100	IHC	Dako	Predilute	1 hour, RT	None
VEGF	WB	Sigma	1:1000	1 hour, RT	N/A

Company	Location
Dako	Carpinteria, CA
Sigma	St. Louis, MO
BD Biosciences	San Diego, CA
Serotec	Raleigh, NC
Cayman	Ann Arbor, MI
AbCam	Cambridge, MA
Cell Signaling	Danvers, MA
Invitrogen/Zymed	San Francisco, CA
Chemicon/Millipore	Temecula, CA/Billerica, MA
Calbiochem (EMD Biosci)	San Diego, CA

All immunohistochemical protocols require blocking sections in 10% serum for 30 minutes (to block nonspecific sites) and in 3% H_2O_2 for 10 minutes (to quench endogenous peroxidase activity). *IHC* indicates immunohistochemistry; *ON*, overnight; *RT*, 25°C; *WB*, Western blot.

*Antigen retrieval method used: 10 mM citrate buffer, pH 6.0, for 10 minutes in microwave and 20 minutes of cool down.

†Antigen retrieval method used: 1 mM EDTA, pH 8, for 10 minutes in microwave and 20 minutes of cool down.

‡Antigen retrieval method used: 0.06% protease (type 24) in Tris buffer for 10 minutes.

§Antigen retrieval method used: enzyme-induced epitope retrieval (EIER) with Digest-all 3 (pepsin; Zymed) for 10 minutes at 37°C. All IHC stains were visualized with diaminobenzidine.

¶CD31 IHC uses a tyramide amplification step; contact authors for detailed protocol.

a combination of methods [39,40] and Tri-Reagent manufacturer's instructions (Molecular Research Center, Inc., Cincinnati, OH). Immediately after euthanizing the mice, tissues were harvested and homogenized with a polytron in 3 ml of 5 M guanidinium thiocyanate buffer containing 50 mM Tris–HCl, 1% laurosyl-sarcosine (Sarkosyl), 10 mM EDTA, pH 7.5, and 1% β-mercaptoethanol. After a brief rest on ice, samples were precipitated 24 to 48 hours at 4°C with seven times the volume of ice-cold 5 M lithium chloride. Samples were then centrifuged for 30 minutes at 12,000*g* (9500 rpm) under 4°C. The supernatant was removed, and the pellet was resuspended in 3 ml of 5 M guanidinium thiocyanate with 1% β-mercaptoethanol followed by 0.1 volume of 2 M sodium acetate, pH 4. The samples were then extracted with 3 to 4 ml of Tri-Reagent following manufacturer's instructions. Samples rested for 5 minutes at room temperature; 0.1 volume of the phase separation reagent 1-bromo-3-chloropropane was then added. Samples were mixed well and allowed to sit at room temperature for 15 minutes, then centrifuged at 12,000*g* (at 4°C). The aqueous layer was removed to a fresh tube, and all extraction steps were repeated. After the second extraction, samples were washed in 2 ml of chloroform, and spun down 15 minutes at 12,000*g* (at 4°C). The top layer was removed, and RNA was precipitated with 6 ml of isopropanol overnight at −20°C. Samples were centrifuged for 15 minutes at 12,000*g*, (at 4°C), and the supernatant was poured off. The RNA pellet was washed once with 75% ethanol made with diethylpyrocarbonate-treated water. A third extraction was performed with Tri-Reagent as previously mentioned, and the aqueous layer was removed to a new tube and precipitated again in 2.5 times the volume of 100% ethanol (overnight at −20°C or 2 hours at −80°C). Samples were spun down at 12,000*g* for 15 minutes and washed once with 1 ml of 75% ethanol. (Samples were transferred to microfuge tubes for the remainder of the procedure.) Samples were centrifuged at 4°C for 15 minutes at maximum speed on a microfuge, washed with 100% ethanol, and recentrifuged. Ethanol was removed, and the pellet was allowed to air dry briefly (~10 minutes) and then resuspended in diethylpyrocarbonate-treated water. An RNAse inhibitor (SUPERaseIn; Ambion, Austin, TX) was added (final concentration is 1 U/μl). Samples were stored at −80°C.

Endogenous COX-2 (a.k.a. Ptgs2*)* Versus *BK5.COX-2 Expression*

*Taq*Man primers and probes were designed to the 5′ and 3′ untranslated regions (UTRs) unique to the mouse endogenous COX-2 gene (*Ptgs2*) and the BK5.COX-2 transgene. Primers and probe specific to exon 7 of *Ptgs2* were used as positive controls because they amplify both the endogenous gene and the transgene from genomic DNA and cDNA (not shown).

Endogenous COX-2 mRNA (Mouse Ptgs2 5′UTR). This assay amplifies a 113-bp product from the endogenous gene and does not amplify the transgene. F-primer: 5′ CAG-TCA-GGA-CTC-TGC-TCA-CGA-A; R-primer: 5′AGC-AGC-ACA-GCT-CGG-AAG-A; probe: 5′-VIC-CGC-CAC-CAC-TAC-TG-MGB-NFQ.

BK5.COX-2 mRNA. This assay amplifies a 72-bp product unique to the transgene and does not amplify *Ptgs2*. F-primer: 5′AAA-GGC-GTT-CAA-CTG-AGC-TGT-AA; R-primer: 5′GGA-GTG-AAT-TGC-TAG-CGT-ATC-GA; probe: 5′-6FAM-CCG-GGC-TGC-AGG-AA-MGB-NFQ.

Total RNA was quantified on a spectrophotometer (ND1000; NanoDrop Technologies, Wilmington, DE), and equal quantities of RNA were used for each sample. The quality of total RNA was verified by analysis on NanoChip with a 2100 Bioanalyzer (Agilent Technologies, Santa Clara, CA). Reverse transcription (RT) of 500 ng of total RNA was carried out in 20-μl reactions with the High-Capacity cDNA Archive Kit (Applied Biosystems, Foster City, CA) according to the manufacturer's recommendations. Antisense primers for *Ptgs2* and BK5.COX-2 (previously mentioned) were substituted at a final concentration of 300 nM for the random primers included in the kit.

Quantitative real-time PCR and RT-PCR (qPCR) were carried out in 25-μl reactions with *Taq*Man FAST Universal PCR Master Mix or SYBR Green Master Mix (Applied Biosystems) and 2-μl template on an ABI Prism 7900HT Sequence Detection System (Applied Biosystems). For qPCR, either 20 ng of genomic DNA or the cDNA generated from RT of 50-ng total RNA was used for each 25-μl reaction. Primer sets were tested by amplification with SYBR green and were selected based on amplification efficiency, dissociation curve analysis, and the presence of single bands of appropriate size visualized on a polyacrylamide gel. Primers were purchased from Integrated DNA Technologies (Coralville, IA), probes from Applied Biosystems.

Synthetic oligos containing the amplicon were purchased from MWG Biotech (High Point, NC). The oligos were diluted serially in a 10-fold dilution series in 25 ng/μl tRNA (Invitrogen, Carlsbad, CA) to generate a standard curve based on the manufacturer's stated concentration and molecular weight. Absolute standard curves were generated using oligo standards ranging from 3.4×10^{12} copies down to 0.34 copies per reaction. For the endogenous COX-2 assay, reaction efficiency was approximately 100% (slope = −3.32, $R = 0.9998$), with a linear range of 340 to 3.4×10^{9} copies. For the BK5.COX-2 assay, reaction efficiency was approximately 100% (slope = −3.32, $R = 0.9997$), with a linear range of 34 to 3.4×10^{8} copies. Sample sizes were as follows: 3-week-old wild type, $n = 4$; 3-week-old transgenic, $n = 4$; 6-month-old wild type, $n = 4$, and transgenic older than 15 weeks, $n = 11$.

PGE_2 Enzyme-Linked Immunosorbent Assay

PGE_2 levels were determined as previously described using a PGE_2 enzyme-linked immunosorbent assay kit from Cayman Chemical (Ann Arbor, MI) [41]. Levels of PGE_2 were determined using the multiple linear regression program on AssayZap (Biosoft, Cambridge, UK) and were expressed as picograms per microgram protein. Experiments were performed in triplicate and repeated three times. Sample sizes for PGE_2 analysis were as follows: wild type, $n = 4$; young transgenic (~4–6 weeks old), $n = 4$; and older transgenic (>15 weeks old), $n = 5$.

Cell Culture and Injections into Nude (Allogeneic) or FVB (Syngeneic) Mice

Minced tumor pieces (1–3 mm) were incubated overnight at 37°C in 200 U/ml collagenase type 1A (Sigma, St. Louis, MO) and suspended in supplemented RPMI 1640 medium (Invitrogen) [42]. After centrifugation, cells were plated in polystyrene flasks. Cultures were observed for colonies with epithelial phenotype; fibroblast overgrowth was minimized by differential trypsinization. Once lines with epithelial morphology were established, medium was changed from high-serum RPMI to DMEM (with high glucose, GlutaMAX, and sodium pyruvate; Invitrogen) supplemented with 5% fetal bovine

serum, insulin (10 μg/ml), and penicillin/streptomycin (100 μg/ml). Cells from one of the epithelial lines (JC102) were injected into the spleens of three 7-week-old nude mice (BALB/cAnCr– *nu/nu*; National Cancer Institute, Frederick, MD) and were allowed to grow for 7 weeks. Cells were injected intraperitoneally (i.p.; JC101 and JC102) or subcutaneously (JC101) into the FVB mice; mice were killed and tissues were collected when the tumors were ~1 cm in diameter or after 30 days.

Chemoprevention Study

Groups of 8 to 12 mice were fed *ad libitum* diets of AIN-76A diet (Research Diets, New Brunswick, NJ) containing celecoxib (LKT Laboratories, St. Paul, MN) at concentrations of 500 (4.5 months), 1000 (3 months), or 1250 ppm (6–10 months). Age- and sex-matched controls were fed AIN-76A (Research Diets) *ad libitum*. Mice were placed on diets at weaning (3–4 weeks) and killed at the end of the feeding periods. Kaplan–Meier survival curves were generated using JMP software (SAS Institute, Cary, NC). For survival analysis, 11 transgenic mice fed 1250 ppm of celecoxib up to 33 weeks were compared with 30 mice fed control diet for the same period.

Statistical Analysis

Statistical differences were performed using analysis of variance (ANOVA) followed by Student's *t* test (one-sided, unequal variance). PGE_2 and endogenous COX-2 expression data were analyzed using Excel (Microsoft Corporation, Redmond, WA). Log-rank analysis of Kaplan–Meier survival data was performed using JMP software (SAS Institute).

Results

Histopathology

Necropsies of newborn and perinatal BK5.COX-2 mice did not reveal any major phenotypic alterations with the exception of a sparse hair coat. At the histologic level, the skin showed slight to moderate inflammation in the dermis and mild hyperplasia of the epidermis. Older mice occasionally developed moderate hyperplasia of the bladder epithelium (data not shown). The first significant pathologic alteration in the pancreas that distinguished the transgenic from wild type mice (Figure 1*A*) was detected at 3 to 4 weeks and consisted of cells with pyknotic nuclei, occasional apoptotic figures, very mild degeneration of the acinar structures coupled with widening of the interlobular spaces, and the presence of a highly vascularized loose connective tissue in the interacinar spaces (Figure 1*B*). Foci of infiltrated mononuclear inflammatory cells were observed among the acini and in the interlobular spaces. Concurrently, acini at discrete sites throughout the pancreas began to undergo a transition to a ductal phenotype, i.e., ductal metaplasia, as evidenced by an increase in the size of the lumen and change in cellular appearance, e.g., loss of zymogen granules and reduction in the amount of cytoplasm. Amylase staining, a marker of acinar differentiation, is retained in early stages of the transition but is completely lost in metaplastic ducts (data not shown). A low but widespread level of necrosis was observed in H&E–stained sections, although no difference was observed in cytoplasmic HMGB1 staining (not shown). Increased proliferation was observed in transitional foci, as evidenced by Ki-67 immunohistochemistry (IHC; Figure 1*C*, *inset*). No difference was seen between Ki-67 staining of 3-week-old wild types and transgenics, because the pancreas was still growing to its adult size (not shown). Full development of the pancreas was complete by 3 months, at which time Ki-67 was almost undetectable in wild type mice (Figure 1*D*, *inset*), whereas extensive Ki-67 staining is evident in transgenics (Figure 1*D*). A high degree of proliferation continued well beyond 3 months in BK5.COX-2 mice (Figure 1*E*).

By 10 weeks, 87% of the transgenic mice develop inflammatory lesions with distinct similarities to human CP [43]. Figure 1*C* shows a representative photomicrograph with characteristic fibrosis, inflammatory cell infiltration, and ductal metaplastic foci. After 10 weeks, an increase in the extent and severity of the pancreatic lesions was observed, reflected by a significant increase in the size of the gland relative to wild type (Figure 1*F*) and the presence of adhesions to abdominal organs (liver, intestine, and spleen) primarily because of the inflammatory process. Microscopically, partial or complete ductal metaplasia of multiple pancreatic lobes was observed, with a significant increase in fibrosis. Lobular architecture of the gland was generally conserved, with a degree of disruption due to extensive fibrosis (Figure 2*A*). At this time point, dysplastic changes were observed in the ductal epithelium in some of the metaplastic foci, consistent with *in situ* premalignant lesions. There was considerable loss of architectural orientation, frequent cellular atypia, increased nuclear to cytoplasmic ratio, and nuclear atypia with prominent nucleoli. Grossly, cystic changes were more noticeable and frequent. Taller mucus-producing cells can be seen in some of the ductal complexes. Lesions with histologic resemblance to mPanINs can be seen as well (Figure 2, *B* and *C*). Necrotic debris is also found in the lumens of many ductal complexes (Figures 2, *D*–*G*).

Lesions of older mice (3–6 months) show histopathologic features that are considered more typical of overt PDAC. Figure 2*D* shows a representative example of a lesion with moderately to well-differentiated ductal structures, an extensive fibroinflammatory reaction, and loss of lobular structure. Mitotic figures were frequently observed, and nuclei were atypical, with prominent nucleoli (Figure 2, *D* and *E*). Cellular atypia and lack of cellular organization, i.e., more haphazard growth of ductal complexes, were also observed (Figure 2, *F* and *G*). As in younger mice, occasional adhesions to other abdominal organs were seen, generally appearing to be the result of the inflammatory process, although some of the adhesions are suggestive of early neoplastic invasion. Figure 2*H* shows an example of such a case, in which abnormal pancreatic cells have adhered and possibly begun to invade through the outer muscularis layers of the intestine. No distant metastases were confirmed, and no signs of peritoneal carcinomatosis were seen. By 6 to 8 months, 100% of the animals had greatly enlarged pancreata and were euthanized as per animal care protocols. Increased volume of the pancreata was frequently, but only partially, a result of cystic fluid (serous) accumulation. Occasionally, mice presented with some degree of ascites as well. At this time point, mean ± SD pancreatic mass was significantly different between wild type and transgenic groups (wild type, 0.28 ± 0.002 g; transgenic, 2.60 ± 1.51 g; $P < .001$; data were obtained after draining cystic fluid). Digestive abnormalities associated with pancreatic insufficiency were not observed, and mice did not show signs of pain. It seemed that at the time of euthanasia, mice still retained sufficient acini to allow normal digestive function.

For controls, 24 wild type mice, from 3 to approximately 50 weeks, were examined histologically. Some of the animals near 1 year were observed to have small infiltrations of lymphocytes in the interstitium (data not shown), which is an incidental lesion commonly seen in aged FVB mice.

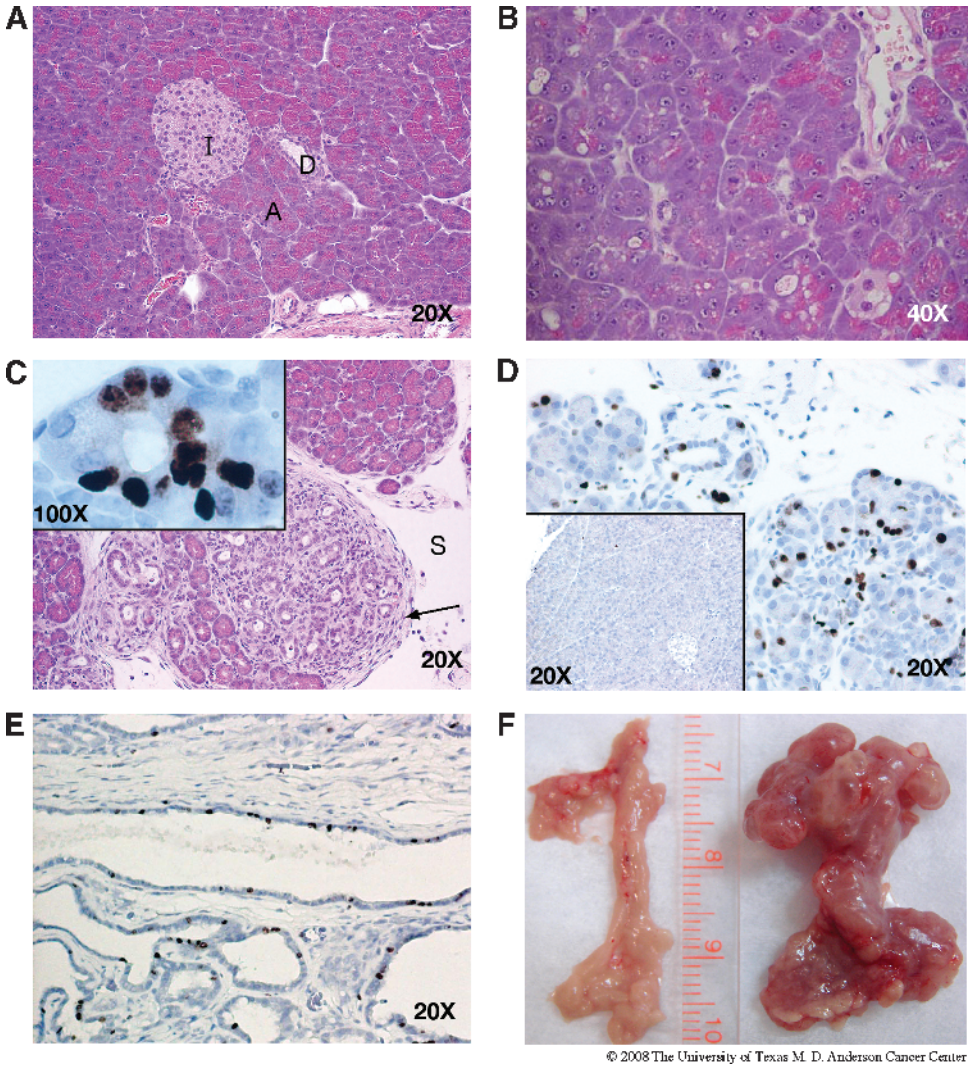

Figure 1. Wild type pancreas and BK5.COX-2 pancreatic lesions. (A) Section of normal wild type FVB pancreas. (B) Early changes in the pancreas of BK5.COX-2 mice. Note prominent nucleoli, acinar atrophy, loss of zymogen granules, and enlargement of interstitial spaces. (C) Section of BK5.COX-2 transgenic pancreas showing formation of ductular complexes (arrow) and an increase in deposition of stroma (S). Inset in (C) is Ki-67 staining of a single acinus in a 3-month-old mouse showing active cellular proliferation of ductlike cells. (D) Comparison of Ki-67 IHC in wild type (inset, D) and transgenic (D) 3-month-old mice. (E) Ki-67 IHC in a more advanced lesion. (F) Gross appearance of the pancreas from 6-month-old wild type (left) and BK5.COX-2 (right) mice.

BK5.COX-2 Cell Lines and Allograft Experiments

To better understand the molecular mechanisms of pancreatic lesion development and to confirm their neoplastic nature, we developed epithelial cell lines from BK5.COX-2 pancreatic lesions, JC101 and 102 (Figure 3, *A* and *B*). JC102 cells were injected in the spleens of three nude mice; tumor growth was assessed after 7 weeks. In two of the mice, metastatic lesions were observed in the liver (Figure 3*C*) and/or in the lung (data not shown). Tumors arising from these cells show COX-2 positivity (Figure 3*D*). JC101 and JC102 cell lines were demonstrated to have the capacity to form aggressive, invasive tumors at a variety of sites. Figure 3*E* shows invasion of cells into skin and muscle adjacent to an i.p. injection site; the inset shows the well-differentiated to moderately differentiated nature of portions of this tumor. Figure 3*F* shows a tumor formed by JC101 cells injected subcutaneously. When injected i.p., tumors grew throughout the peritoneal cavity, invading organs such as intestine, pancreas and liver (Figure 3, *G–I*). These tumors, in general, tended to be less well differentiated, i.e., showing fewer ductal structures. Cell lines JC101 and 102 have been serially passaged through i.p. injection to wild type FVB mice; cells retain both *in vitro* and tumorigenic characteristics of the original cell lines.

Transgene Expression

Because BK5.COX-2 mice presented with primarily a pancreatic phenotype, transgene expression was analyzed in detail in the pancreas. In 3-week-old transgenic mice, only normal ducts and low numbers of acinar cells are strongly positive for COX-2. As expected, islets in both wild types and transgenics show weak COX-2 expression (Figure 4, *A* and *B*). As the transgenic mice aged, COX-2 expression increased, mainly in ducts (metaplastic and normal) and in acinar cells (Figure 4*C*). Because of this unexpected acinar expression, and because the construct was prepared without a molecular tag, it was necessary to verify the location of transgene expression in the pancreas through additional means. To accomplish this, we

used a mouse model in which the BK5 promoter drives the expression of CFP (BK5.CFP mice) to identify those cells in which the BK5 promoter is active (and therefore COX-2 transgene-positive) before onset of pathologic changes. CFP and BK5 expression are coincident in this model; CFP fluorescence was observed only in the ductal epithelium of the BK5.CFP mouse pancreas. No fluorescence was detected in other pancreatic cell types (Figure 4*D*).

Endogenous COX-2 Expression

On the basis of acinar cell COX-2 expression, we hypothesized that the transgene was producing PGs, and possibly other cytokines, that caused expression of the endogenous COX-2 gene. This was verified through quantitative RT-PCR of pancreas samples from WT and transgenic mice (Figure 4*E*). The endogenous gene is expressed at slightly elevated levels in the young transgenics (3 weeks) and is greatly, although variably, increased in pancreata harvested from older transgenics. Variability is likely due to sample heterogeneity, as the ratio of stroma to epithelium in lesions can vary considerably. The level of endogenous COX-2 differs significantly between transgenics >15 weeks and all other groups (Figure 4*E*).

PGE_2 Levels

To confirm transgene functionality, we analyzed PGE_2 in pancreata from normal wild type mice, young transgenics with mild disease, and more severely affected older transgenics. Levels of PGE_2 were elevated in young transgenic mice and significantly increased with age and lesion severity (Figure 4*F*). Levels were more variable in advanced lesions due to heterogeneity present in those samples.

Markers of Normal and Diseased Pancreas

Islet beta cells were positive for insulin in both the wild type and transgenic mice (Figure 5*A*). α-Smooth muscle actin (α-SMA), a common marker of activated pancreatic stellate cells (PaSCs), was increased in the stroma of BK5.COX-2 pancreata (Figure 5*B*). Elastase expression was observed in the acinar cell compartment as expected but was also seen in early ductal structures (Figure 5*C*).

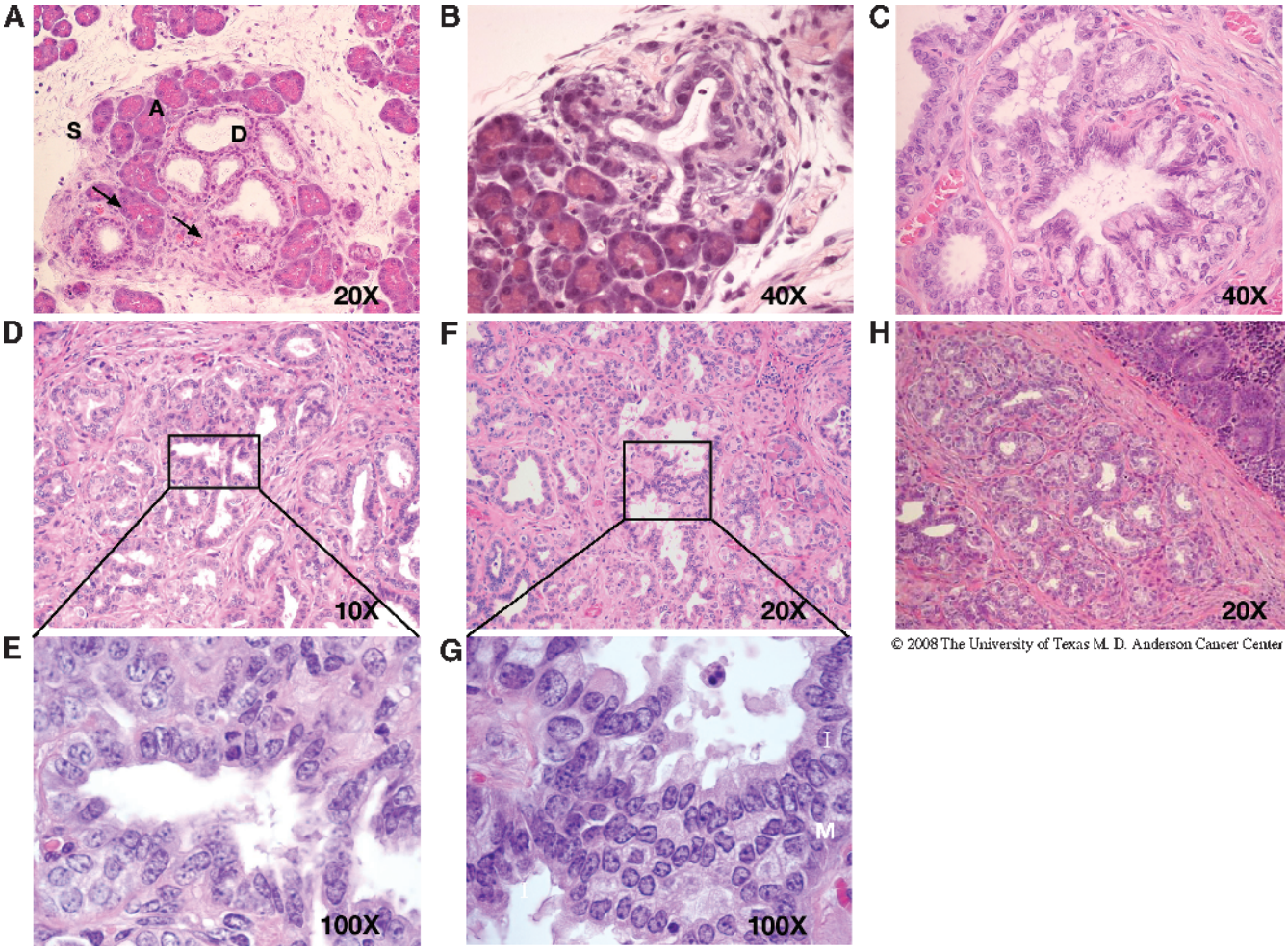

Figure 2. Increasing metaplastic and dysplastic progression in the BK5.COX-2 pancreas. (A) Pancreas from a 3-month-old BK5.COX-2 with changes histologically similar to CP including metaplastic ductal cells ("D"), mild nuclear atypia, increased reactive stroma ("S"), and the presence of numerous small vessels (arrows). Note unaffected acini ("A") in the field. (B and C) Example of "mPanIN"–like lesion in BK5.COX-2 pancreas. (D–G) Higher-grade dysplastic changes in BK5.COX-2 pancreas. Higher magnifications of the boxed areas in D and F are shown in E and G. Acini have been replaced by abnormal ductal structures, consisting of cells with significant atypia. Note cellular disorganization and presence of necrotic debris in lumens of metaplastic ducts. An example of an adhesive (and possibly invasive) lesion affecting the intestine is shown in H.

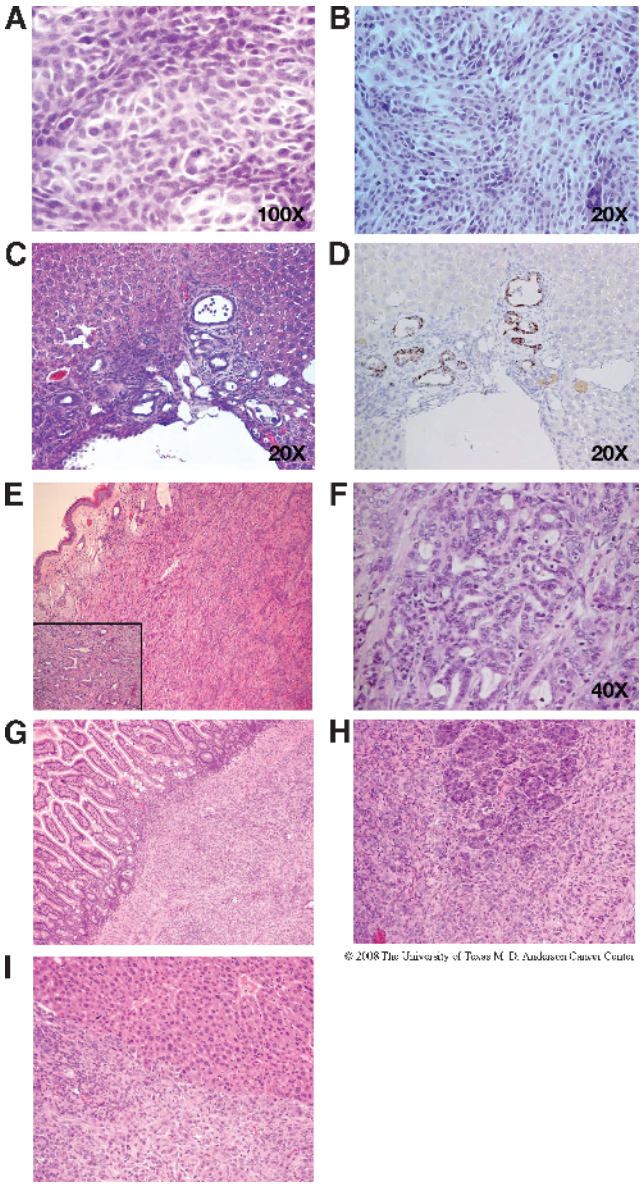

Figure 3. Allograft experiments. H&E–stained sections of JC101 (A) and JC102 (B) cells grown on a chamber slide. H&E–stained section of the liver metastasis (C) of JC102 cells injected into the spleen. (D) Immunohistochemistry for COX-2 expression in metastasis shown in (C). H&E–stained section of tumor arising near the injection site of i.p.–injected JC102 cells (E). Note invasion to muscle and skin. The inset in E shows a portion of the same tumor that is well to moderately differentiated. (F) Tumor arising from subcutaneously injected JC101 cells. (G–I) Tumors arising from i.p.–injected JC101 or 102 cells. Tumors invading the small intestine (G), normal pancreas (H), and liver (I) are shown.

Ductal complexes lose elastase expression as they proliferate. An identical staining pattern is observed with amylase IHC (data not shown). Keratin 19 (K19) is an intermediate filament protein found in pancreatic ducts and is frequently used to confirm a true ductal phenotype [44]. Keratin 19 staining is widespread in BK5.COX-2 ductal complexes, indicative of a ductal, as opposed to acinar, phenotype (Figure 5*D*).

β-Catenin and E-cadherin have critical roles in adhesion and signaling and are frequently dysregulated and/or expressed in aberrant patterns in both preneoplastic lesions and neoplasia. In BK5.COX-2 mice, cytoplasmic β-catenin levels increase in comparison to wild type, which have a typical membrane-bound pattern of β-catenin staining (Figure 5*E*). A similar pattern is observed with E-cadherin staining (Figure 5*F*). The S100 proteins are a group of calcium-binding proteins having numerous effects on cell behavior; they are often overexpressed in cancer and may have prognostic value [45]. Using a pan-S100 antibody, we observed a distinct increase in S100 staining in BK5.COX-2 transgenic pancreas (Figure 5*G*). Pancreatic ductal adenocarcinoma frequently shows a dysregulated production of mucins [46]. Alcian blue staining, used for the detection of mucins, is much more prominent in BK5.COX-2 lesions *versus* controls (Figure 5*H*). Positive staining for PAS and mucicarmine, additional indicators of mucins, were also observed in transgenic lesions (data not shown).

An increase in vessel number in the stroma of transgenic lesions was observed in H&E–stained sections and was confirmed by immunostaining for CD31 (Figure 5*I*). Vascular endothelial growth factor (VEGF) is another indicator of an angiogenic response; immunoblot analysis showed up-regulation of VEGF in transgenic pancreata (not shown). In the pancreas, matrix metalloproteinase 7 (MMP-7) is involved in acinar-to-ductal transdifferentiation and is up-regulated in most human PDAC [47]. Matrix metalloproteinase 9 (MMP-9; gelatinase B) is involved in the remodeling of extracellular matrix in normal and disease processes, and stromal expression of MMP-9 is necessary for the angiogenesis and progression of tumors in a nude mouse model using orthotopically implanted pancreatic cancer cells [48,49]. In our model, MMP-9 is elevated in transgenic pancreata as determined by immunoblot analysis (not shown). Matrix metalloproteinase 7 expression was evaluated by IHC; areas of positivity are seen in both stroma and acinar cells undergoing metaplastic change (Figure 5*J*).

Inflammatory Cell Markers

A range of cells typical of inflammatory responses is observed in BK5.COX-2 lesions. The earliest abnormal pancreata have an influx of neutrophils, and later macrophages, as verified by Ly6G (Gr-1) and S100A9 IHC (Figure 6, *A* and *B*), respectively. More advanced lesions generally possessed numerous B and T lymphocytes, often present in large clusters (Figure 6, *C* and *D*). B- and T-cell identities were verified by CD45R (Figure 6*C*) and CD3 (Figure 6*D*) IHC, respectively. Toluidine blue histochemistry demonstrated the presence of mast cells (Figure 6*E*).

Celecoxib Feeding Studies

To demonstrate that pancreatic lesions in BK5.COX-2 mice were due to high levels of PG synthesized by COX-2, transgenic mice were fed diets containing celecoxib (500–1250 ppm), a selective COX-2 inhibitor. Kaplan–Meier analysis revealed significant differences between groups (Figure 7*A*). None of the mice fed celecoxib showed any evidence of pancreatic lesions (Figure 7*B*). Several mice on the highest dose (1250 ppm) died because of gastrointestinal toxicity, but none had pancreatic abnormalities. The lower doses of celecoxib (500 and 1000 ppm) proved equally effective at preventing lesions with significantly less toxicity (data not shown). As noted previously, mice on the control diet were euthanized in compliance with animal care regulations, generally due to the extensive enlargement of the pancreas due to cystic fluid accumulation/fibrosis leading to compression/dysfunction of other organs.

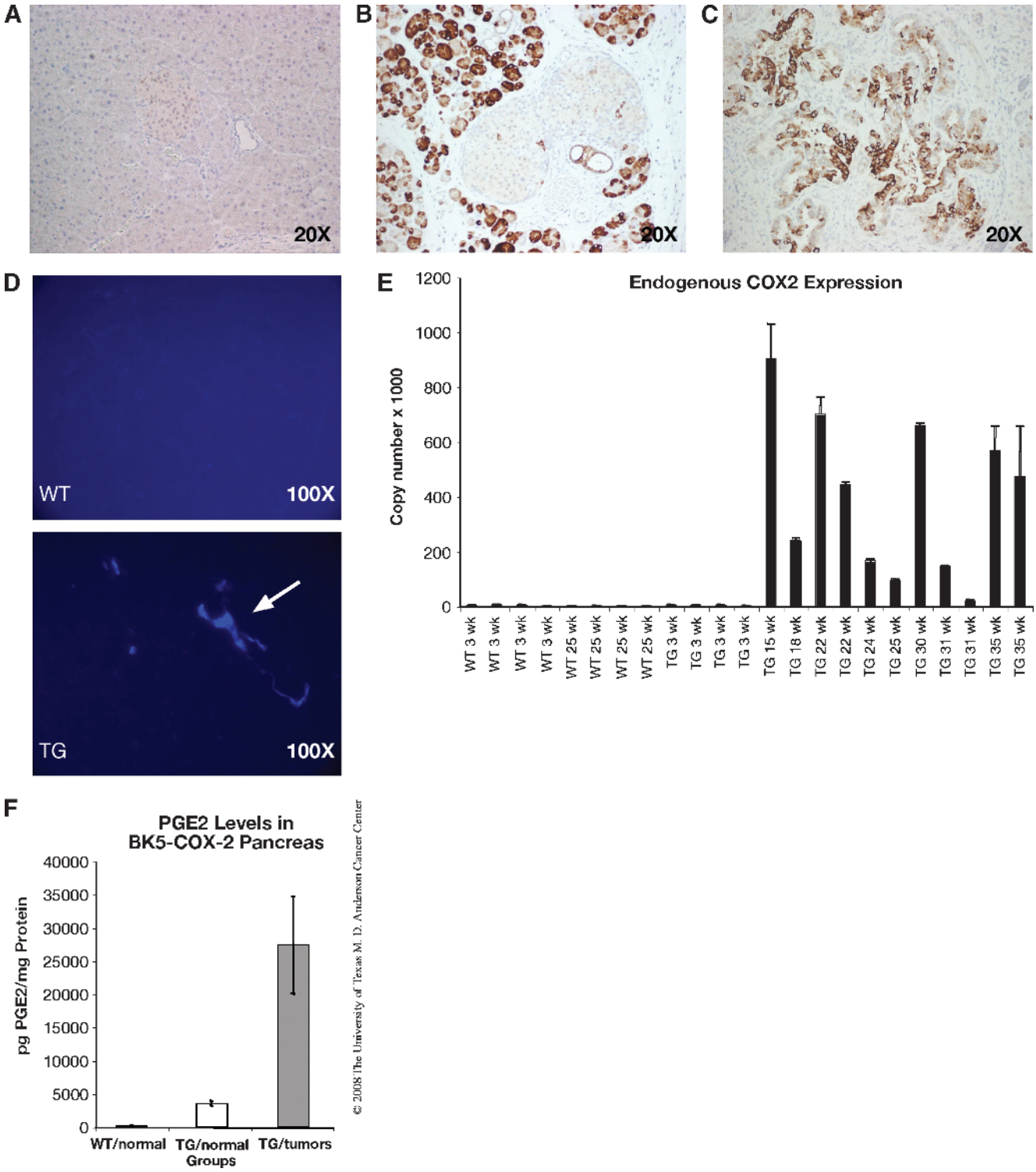

Figure 4. COX-2 transgene expression in BK5.COX-2 mice and BK5.CFP immunofluorescence. Cyclooxygenase-2 IHC on 3-week-old wild type FVB (A) and BK5.COX-2 transgenic mice (B). Cyclooxygenase-2 IHC in a more advanced BK5.COX-2 pancreatic lesion (C). BK5.CFP immunofluorescence in wild type (insert in D) and transgenic mice (D) demonstrating keratin 5 expression in the ductal compartment only. Quantitative RT-PCR results (E) showing increased mRNA for endogenous COX-2. Data are presented such that each bar represents a single animal. When grouped for analysis (ANOVA), significant differences exist between groups ($P = .002$); transgenic tumors (including all transgenics 15 weeks or older) differed significantly from all other groups (P values $< .0005$ for comparisons with 3-week-old wild type, 3-week-old transgenic, and 6-month-old wild type groups (mean ± SD for groups: 3-week-old wild type, 3.175 ± 1.56; 3-week-old transgenic, 3.575 ± 0.665; 6-month-old wild type, 1.1 ± 0.688; and older transgenics/tumors, 402.1/287.96). PGE_2 levels (F) in wild type FVB, prelesion (young) transgenic mouse pancreas, and premalignant transgenic pancreatic lesions. Differences between groups are significant; ANOVA for all groups, $P = .005$; significant differences were also detected between wild type and young transgenic ($P = .001$), between wild type and lesion ($P = .01$), and between young transgenic and transgenic lesion ($P = .015$). Mean ± SD for groups: wild type, 229 ± 95.10; young transgenic, 3632.25 ± 708.17; and lesion, 27,466.2 ± 16,408.02.

Discussion

We present data supporting a model (Figure 8) of PGE_2-driven neoplasia in which transgene-expressing ductal cells serve as the initial source of PGE_2, subsequently causing paracrine and autocrine upregulation of endogenous COX-2 in acinar and normal ductal cells, respectively. Whereas additional inflammatory mediators (e.g., tumor necrosis factor α, interleukin 1β) are likely to be involved in the process, PGE_2 elevation in transgenic pancreata is key in establishing a proinflammatory environment capable of initiating and supporting metaplastic and dysplastic changes. All mice develop pancreatic inflammation and metaplasia characteristic of human CP, subsequently followed by development of highly dysplastic lesions with features of

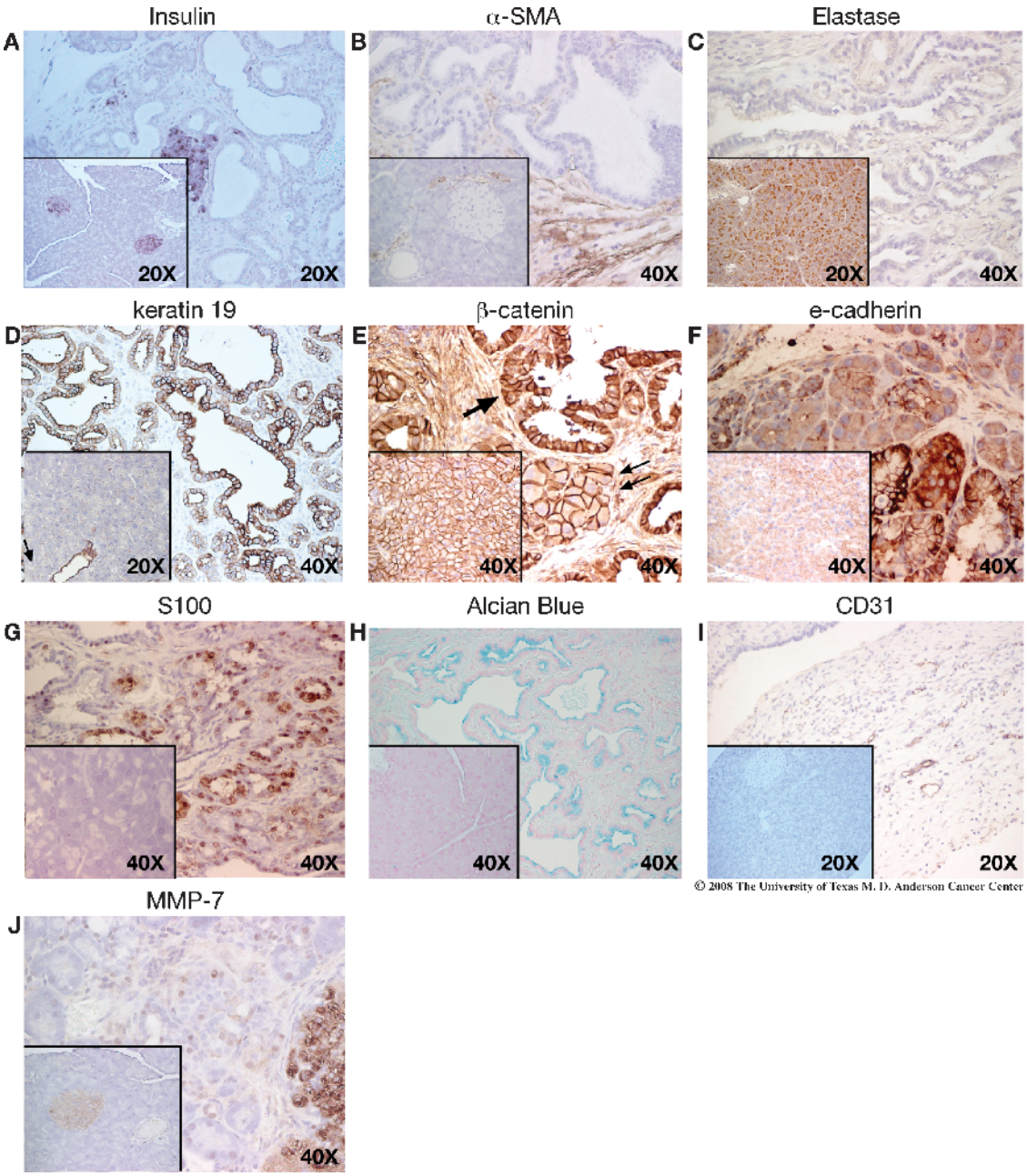

Figure 5. Altered protein expression in BK5.COX-2 mouse pancreata (large images) compared to wild type (insets). (A) Insulin expression is normal in both wild type and transgenic mice. (B) α-Smooth muscle actin expression is increased in BK5.COX-2 transgenics, reflecting activation and expansion of stellate cells. (C) Elastase staining is restricted to acini in wild type mice but appears in metaplastic ductal structures as well in transgenics. (D) Keratin 19, a marker of ductal differentiation, shows extensive staining in transgenic lesions, whereas only normal ducts stain positive (arrow) in wild type mice. (E) β-Catenin staining is restricted to the cytoplasmic membrane in wild types but becomes more strongly expressed in the cytoplasm of cells making up transgenic lesions. (F) E-Cadherin shows a pattern similar to that observed with β-catenin (see E). (G) S100 protein is strongly expressed in transgenic lesions, primarily in epithelial cells. (H) Alcian blue staining reveals the presence of mucin in the lumens of ductal lesions of transgenics; little staining is seen in wild type mice. (I) The expanding stroma in BK5.COX-2 pancreata is well vascularized as verified by CD31 staining. (J) Matrix metalloproteinase 7 staining has been associated with acinar–ductal metaplasia and is more highly expressed in BK5.COX-2 pancreatic lesions.

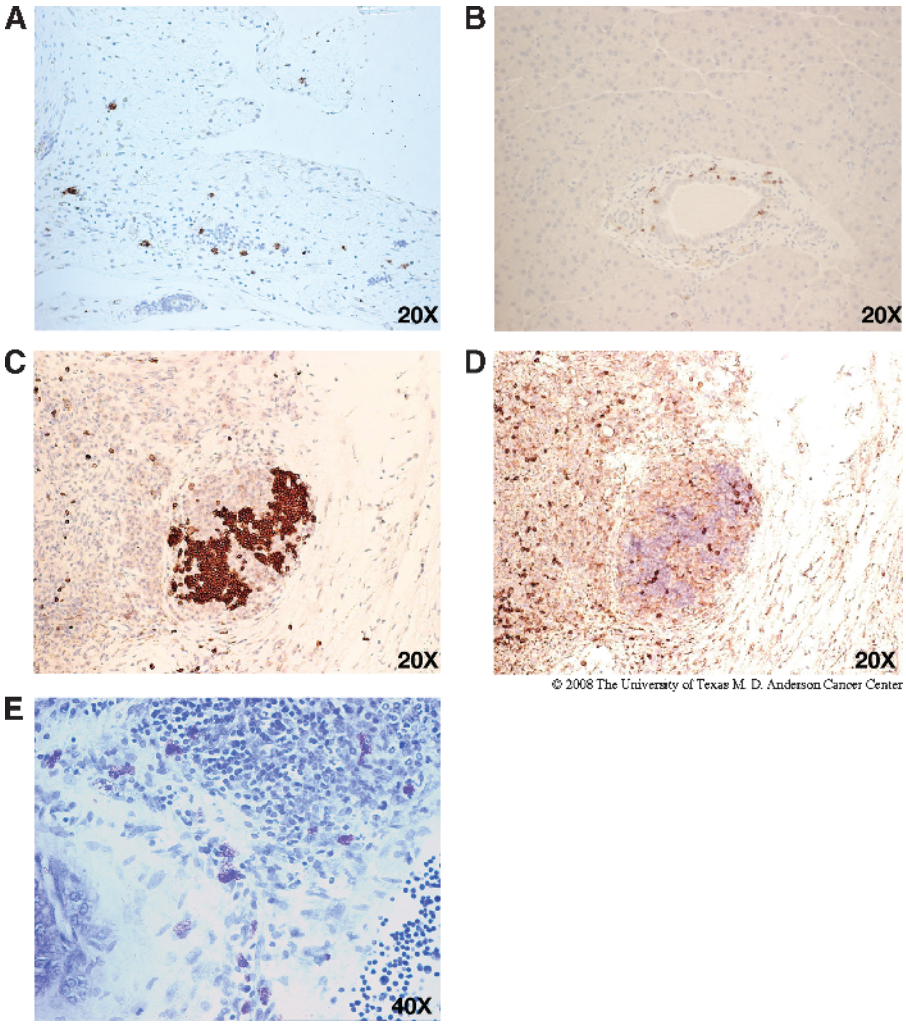

Figure 6. Inflammatory cells in BK5.COX-2 lesions. (A) The earliest inflammatory cells observed in the BK5.COX-2 pancreata are Ly6G-positive neutrophils. Macrophages appear slightly later, here identified by S100A9 IHC (B). (C and D) B and T lymphocytes appear as lesions progress, often forming large clusters of cells. B cells are identified using a CD45R antibody (C) and T cells with CD3 antibody (D). Mast cells occur frequently in the stroma of transgenic lesions; here, they are identified by toluidine blue (E).

frank adenocarcinoma, such as the presence of mucins and nuclear atypia. Increased numbers of fibroblast-like stromal cells expressing α-SMA occur in our model, representing activated PaSCs. PaSCs normally make up only 4% of the normal pancreas and have a retinol storage function in their quiescent state [50]. In inflammatory responses, they become activated and undergo changes leading to deposition of high levels of extracellular matrix components and fibrosis observed in pancreatitis and PDAC [51]. Immunocytes are also found in the

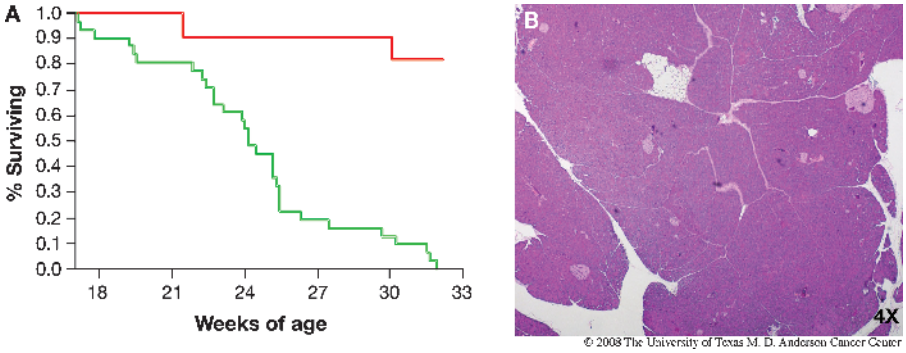

Figure 7. Prostaglandins drive the development of pancreatic inflammation and premalignant lesions in BK5.COX-2 mice. (A) Kaplan–Meier survival curve of mice fed 1250 ppm of celecoxib for 33 weeks ($P < .0001$). The incidence of pancreatic lesions was zero in the celecoxib-fed group (red line); see text for details. (B) Hematoxylin and eosin–stained section of pancreas in a transgenic mouse fed the celecoxib diet.

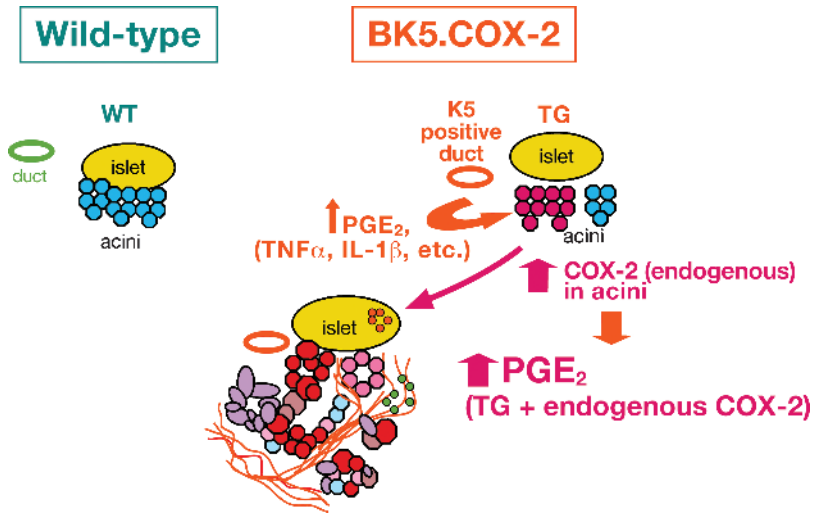

Figure 8. Working model of pancreatic tumorigenesis in BK5.COX-2 mice. Transgene-produced PGE_2 from the phenotypically normal transgene-positive ductal epithelium stimulates expression either directly [through signaling through PGE_2 receptors (EP)] or indirectly [through up-regulation of additional inflammatory mediators, e.g., tumor necrosis factor α (TNFα), interleukin 1β (IL-1β), interleukin 6 (IL-6)] of the endogenous COX-2 gene in surrounding acinar cells, causing an even greater increase in tissue PGs, leading to concomitant inflammation and acinar–ductal metaplasia. In this model, a CP-like state ultimately leads to development of high-grade dysplasia with many cytologic and histologic features of overt PDAC.

lesions, including neutrophils, macrophages, mast cells, and B and T lymphocytes, further indicating the inflammatory nature of this model.

Acinar-to-ductal metaplasia is a key feature of BK5.COX-2 lesions and has been described in other genetically modified mouse models, most notably, the Ela-RAS^{G12D} (elastase promoter–driven mutant Ras [52]) and Ela-TGFα-hGH (elastase promoter–driven transforming growth factor α) [32]. Metaplasia occurs in response to chronic tissue injury or stress and is seen in several well-characterized human neoplastic conditions, e.g., Barrett metaplasia of the esophagus, a precursor lesion for esophageal cancer caused by chronic gastroesophageal reflux [53]. Morphologic changes triggered by the exposure of acinar cells to unusual stress (culture conditions, inflammatory mediators) seems to confer greater resistance to further injury or death, and greater regenerative potential. The enhanced proliferative response, including expansion of the stromal compartment, is also typical of injured/healing tissue. In the BK5.COX-2 model, chronic inflammation and the accompanying regenerative response lead to metaplastic changes similar to those seen in human CP. Pancreatic acinar–ductal transdifferentiation has also been convincingly demonstrated in both tissue culture and *in vivo* models, and it is thought that this metaplastic change produces a population of cells with greater proliferative potential that may act as facultative stem cells [11,54,55]. In further support of the link between metaplasia and hyperplasia in the pancreas, a recent study by Zhu et al. [13] suggests that active cell division does not take place until acinar cells have undergone metaplastic change to a ductal cell–like phenotype. In human pancreas, evidence of a "transitional zone" with co-occurrence of tubular complexes and low-grade PanIN (1A) suggests the existence of a progression sequence from tubular complexes to PanIN formation [18]. In addition, a recent review of the literature favors the idea that the variety of histologic complexity observed in numerous transgenic mouse models is in fact consistent with the heterogeneity seen in human PDAC [56]. A study by Strobel et al. [57] used lineage tracing of acinar cells and found that in a cerulein model of CP, certain subsets of metaplastic ductal lesions seem to arise from transdifferentiation of acinar cells while others do not. Although these data are intriguing, it is possible that the mechanisms behind metaplastic events are model-specific. The cerulein pancreatitis models have been well studied, but there is concern that they do not reflect human CP accurately [58,59]. Not all forms of human CP seem to share the same pathogenetic mechanisms, and there are important differences between rodents and humans in terms of molecular signaling on which the cerulein model is based [60]. Although there are multiple mechanisms by which metaplasia may occur (for a review, see Slack [10]), the ductal complexes observed in the BK5.COX-2 pancreas do not seem to be due to replacement of dying acinar cells by rapid proliferation of the ductal compartment. Although we cannot strictly rule out the co-occurrence of different metaplastic processes, we believe that we are observing a significant degree of acinar-to-ductal transdifferentiation. This view is supported by the observation that extensive simultaneous death of acinar cells is not seen and by the expression patterns of amylase and K19. Because PGE_2 can confer both survival and growth advantages, it may act both to prevent apoptosis and to promote proliferation.

The precise molecular pathways/mechanisms impacted in the BK5.COX-2 model are still incompletely described, but multiple processes are potentially involved, e.g., macromolecular damage either because of lipid peroxidation or reactive oxygen species (including alterations in DNA) or because of chronic activation of growth factor receptors. We assessed several markers frequently associated with CP and/or neoplastic transformation using IHC. Stronger cytoplasmic expressions of β-catenin and E-cadherin, both of which can be dysregulated in human pancreatic lesions, were observed and suggest alterations in cell adhesion properties and perhaps Wnt signaling [61,62]. Matrix metalloproteinases have been associated with increased invasive behavior and poor prognosis in other studies [47,49]. S100 proteins signal through the multiligand receptor RAGE (receptor for advanced glycation end products) [63]. When present at lower tissue concentrations, RAGE ligands activate repair mechanisms, whereas at elevated levels, they are associated with chronic tissue injury. It is thought

that in stressful environments such as chronically inflamed tissue, ligands for RAGE may be present as higher-order oligomers, possibly overwhelming normal resolution mechanisms [63]. Up-regulation of S100 proteins also suggests changes in calcium signaling, which can affect many aspects of cell behavior, including cell cycling and differentiation [45].

In spite of the presence of molecular markers frequently associated with more aggressive neoplastic behavior, BK5.COX-2 tumors showed only occasional invasion and no identifiable metastases. Although we were unable to unequivocally demonstrate metastases originating from spontaneous lesions, cell lines derived from primary lesions were shown to be tumorigenic, suggesting the presence of additional genetic or epigenetic changes within the cells. Most PDAC cases in humans show mutations in K-*ras* [64]; however, mutation-specific sequencing failed to show any evidence of signature K-*ras* mutations in BK5.COX-2 tumors (not shown). Because COX-2 up-regulation is downstream of ras activation, our model may bypass the "need" for K-*ras* mutation [65]. Activated ras, however, was detected in BK5.COX-2 cell lines used for injection experiments (data not shown). Ras activation may reflect a critical change responsible for the more aggressive behavior of tumors arising from the cell lines, although it is still possible that additional mutations may have been selected for in the process of deriving the lines from spontaneous tumors. Interestingly, a recent article demonstrated that in adult mice expressing mutant ras ($K\text{-}Ras^{G12V}$), inflammatory changes are necessary for the full development of neoplastic changes [14].

An interesting feature seen in most spontaneously occurring BK5.COX-2 pancreatic lesions is the presence of cystic changes, a feature shared with several other mouse models of pancreatic disease [32,66–68], giving the tumors a gross resemblance to serous cystadenoma/adenocarcinoma [69]. Although the lesions appear grossly like these neoplasms, microscopically, BK5.COX-2 lesions show much more dramatic dysplasia, with histologic characteristics more in line with ductal adenocarcinoma. Newer imaging techniques have lead to more frequent discovery of pancreatic cysts in humans, and a number of recent articles have addressed the significance of cystic lesions in pancreatitis and PDAC [70–74]. Although observed less frequently in humans than solid neoplasms, cystic variants of many lesions occur, some with malignant features [71]. Distinguishing benign cysts from those with malignant potential is a diagnostic challenge, particularly against a background of CP [73,75]. Although the full significance of pancreatic cysts is not known, there are data suggesting an increased risk for PDAC in persons with pancreatic cystic changes [72].

In a recent publication [31], a COX-2 transgenic mouse generated on the NMRI background displays some of the characteristics of our model but with critical differences. Similarities exist in terms of the histopathology of ductal lesions, but a lower percentage of these mice are affected (15% at 6 months; 30% of 12 months), and latency is greatly increased (lesions take two to three times longer to manifest themselves). The differences between this model and our own could be advantageous in efforts to distinguish important genetic or epigenetic cofactors influencing the progression of pancreatic disease.

Identification of early, premaligant changes is critical for the development of improved prevention or intervention approaches. There has been mixed success using COX-2 selective inhibitors such as celecoxib in preclinical/xenograft models of pancreatic cancer, with some groups reporting inhibition of angiogenesis or growth factor–associated signaling [76–78] and others showing no effect [79]. Unfortunately, the efficacy of celecoxib as an adjuvant to standard chemotherapeutic protocols has been quite limited [79–82], further highlighting the need for the earlier detection of preneoplastic lesions and a stronger focus on prevention. A number of studies have demonstrated causal links between tobacco and/or alcohol use and pancreatic inflammation and neoplasia [4,5,8]. Cyclooxygenase-2 is frequently found to be elevated in these studies and can be considered an important biomarker in CP and PDAC. As an example, a recent study by Schuller et al. [83] employed a radiolabeled drug to help identify precancerous lesions that significantly overexpressed COX-2 in 4-(methylnitrosamino)-1-(3-pyridyl)-1-butanone–treated hamster tissues (liver, lung, and pancreas). In addition, COX-2 inhibition has been shown to limit the progression of mPanINs in the $Kras^{G12D}$ model [84]. We believe that the BK5.COX-2 model has attributes that will make it a valuable model in furthering our understanding of how unresolved inflammatory processes can initiate premalignant changes linked to pancreatic cancer and how such changes can be prevented. Data obtained from this and other related models should broaden our understanding of the complex relationship between inflammation and pancreatic cancer [12–14,31].

Acknowledgments

The authors thank Weidan Peng and Yunhua Bao (Lankenau), Nancy W. Otto, and Kelly Kochan (Science Park) and the personnel at the Science Park Animal Research Facility for expert technical assistance. Joi Holcombe (Science Park) provided excellent assistance with graphics.

References

[1] Lowenfels AB, Maisonneuve P, DiMagno EP, Elitsur Y, Gates LK Jr, Perrault J, and Whitcomb DC (1997). Hereditary pancreatitis and the risk of pancreatic cancer. International Hereditary Pancreatitis Study Group. *J Natl Cancer Inst* **89**, 442–446.

[2] Farrow B, Sugiyama Y, Chen A, Uffort E, Nealon W, and Mark Evers B (2004). Inflammatory mechanisms contributing to pancreatic cancer development. *Ann Surg* **239**, 763–769; discussion 769–771.

[3] Hezel AF, Kimmelman AC, Stanger BZ, Bardeesy N, and Depinho RA (2006). Genetics and biology of pancreatic ductal adenocarcinoma. *Genes Dev* **20**, 1218–1249.

[4] Maisonneuve P, Lowenfels AB, Mullhaupt B, Cavallini G, Lankisch PG, Andersen JR, Dimagno EP, Andren-Sandberg A, Domellof L, Frulloni L, et al. (2005). Cigarette smoking accelerates progression of alcoholic chronic pancreatitis. *Gut* **54**, 510–514.

[5] Schuller HM (2002). Mechanisms of smoking-related lung and pancreatic adenocarcinoma development. *Nat Rev Cancer* **2**, 455–463.

[6] Nkondjock A, Krewski D, Johnson KC, and Ghadirian P (2005). Dietary patterns and risk of pancreatic cancer. *Int J Cancer* **114**, 817–823.

[7] Jee SH, Ohrr H, Sull JW, Yun JE, Ji M, and Samet JM (2005). Fasting serum glucose level and cancer risk in Korean men and women. *JAMA* **293**, 194–202.

[8] Stolzenberg-Solomon RZ, Graubard BI, Chari S, Limburg P, Taylor PR, Virtamo J, and Albanes D (2005). Insulin, glucose, insulin resistance, and pancreatic cancer in male smokers. *JAMA* **294**, 2872–2878.

[9] Jura N, Archer H, and Bar-Sagi D (2005). Chronic pancreatitis, pancreatic adenocarcinoma and the black box in-between. *Cell Res* **15**, 72–77.

[10] Slack JM (2007). Metaplasia and transdifferentiation: from pure biology to the clinic. *Nat Rev Mol Cell Biol* **8**, 369–378.

[11] Means AL, Meszoely IM, Suzuki K, Miyamoto Y, Rustgi AK, Coffey RJ Jr, Wright CV, Stoffers DA, and Leach SD (2005). Pancreatic epithelial plasticity mediated by acinar cell transdifferentiation and generation of nestin-positive intermediates. *Development* **132**, 3767–3776.

[12] Archer H, Jura N, Keller J, Jacobson M, and Bar-Sagi D (2006). A mouse model of hereditary pancreatitis generated by transgenic expression of R122H trypsinogen. *Gastroenterology* **131**, 1844–1855.

[13] Zhu L, Shi G, Schmidt CM, Hruban RH, and Konieczny SF (2007). Acinar cells contribute to the molecular heterogeneity of pancreatic intraepithelial neoplasia. *Am J Pathol* **171**, 263–273.

[14] Guerra C, Schuhmacher AJ, Canamero M, Grippo PJ, Verdaguer L, Perez-Gallego L, Dubus P, Sandgren EP, and Barbacid M (2007). Chronic pancreatitis

is essential for induction of pancreatic ductal adenocarcinoma by K-Ras oncogenes in adult mice. *Cancer Cell* **11**, 291–302.
[15] Hruban RH, Adsay NV, Albores-Saavedra J, Anver MR, Biankin AV, Boivin GP, Furth EE, Furukawa T, Klein A, Klimstra DS, et al. (2006). Pathology of genetically engineered mouse models of pancreatic exocrine cancer: consensus report and recommendations. *Cancer Res* **66**, 95–106.
[16] Schmid RM (2002). Acinar-to-ductal metaplasia in pancreatic cancer development. *J Clin Invest* **109**, 1403–1404.
[17] Hruban RH, Takaori K, Klimstra DS, Adsay NV, Albores-Saavedra J, Biankin AV, Biankin SA, Compton C, Fukushima N, Furukawa T, et al. (2004). An illustrated consensus on the classification of pancreatic intraepithelial neoplasia and intraductal papillary mucinous neoplasms. *Am J Surg Pathol* **28**, 977–987.
[18] Esposito I, Seiler C, Bergmann F, Kleeff J, Friess H, and Schirmacher P (2007). Hypothetical progression model of pancreatic cancer with origin in the centroacinar–acinar compartment. *Pancreas* **35**, 212–217.
[19] Bockman DE, Guo J, Buchler P, Muller MW, Bergmann F, and Friess H (2003). Origin and development of the precursor lesions in experimental pancreatic cancer in rats. *Lab Invest* **83**, 853–859.
[20] Schmid RM, Kloppel G, Adler G, and Wagner M (1999). Acinar–ductal–carcinoma sequence in transforming growth factor-alpha transgenic mice. *Ann NY Acad Sci* **880**, 219–230.
[21] Greten FR, Wagner M, Weber CK, Zechner U, Adler G, and Schmid RM (2001). TGF alpha transgenic mice. A model of pancreatic cancer development. *Pancreatology* **1**, 363–368.
[22] FitzGerald GA (2003). COX-2 and beyond: approaches to prostaglandin inhibition in human disease. *Nat Rev Drug Discov* **2**, 879–890.
[23] Dannenberg AJ, Lippman SM, Mann JR, Subbaramaiah K, and DuBois RN (2005). Cyclooxygenase-2 and epidermal growth factor receptor: pharmacologic targets for chemoprevention. *J Clin Oncol* **23**, 254–266.
[24] Yip-Schneider MT, Barnard DS, Billings SD, Cheng L, Heilman DK, Lin A, Marshall SJ, Crowell PL, Marshall MS, and Sweeney CJ (2000). Cyclooxygenase-2 expression in human pancreatic adenocarcinomas. *Carcinogenesis* **21**, 139–146.
[25] Schlosser W, Schlosser S, Ramadani M, Gansauge F, Gansauge S, and Beger HG (2002). Cyclooxygenase-2 is overexpressed in chronic pancreatitis. *Pancreas* **25**, 26–30.
[26] Crowell PL, Schmidt CM, Yip-Schneider MT, Savage JJ, Hertzler DA II, and Cummings WO (2006). Cyclooxygenase-2 expression in hamster and human pancreatic neoplasia. *Neoplasia* **8**, 437–445.
[27] Liu CH, Chang SH, Narko K, Trifan OC, Wu MT, Smith E, Haudenschild C, Lane TF, and Hla T (2001). Overexpression of cyclooxygenase-2 is sufficient to induce tumorigenesis in transgenic mice. *J Biol Chem* **276**, 18563–18569.
[28] Klein RD, Van Pelt CS, Sabichi AL, Dela Cerda J, Fischer SM, Furstenberger G, and Muller-Decker K (2005). Transitional cell hyperplasia and carcinomas in urinary bladders of transgenic mice with keratin 5 promoter–driven cyclooxygenase-2 overexpression. *Cancer Res* **65**, 1808–1813.
[29] Muller-Decker K, Neufang G, Berger I, Neumann M, Marks F, and Furstenberger G (2002). Transgenic cyclooxygenase-2 overexpression sensitizes mouse skin for carcinogenesis. *Proc Natl Acad Sci USA* **99**, 12483–12488.
[30] Muller-Decker K, Berger I, Ackermann K, Ehemann V, Zoubova S, Aulmann S, Pyerin W, and Furstenberger G (2005). Cystic duct dilatations and proliferative epithelial lesions in mouse mammary glands upon keratin 5 promoter–driven overexpression of cyclooxygenase-2. *Am J Pathol* **166**, 575–584.
[31] Muller-Decker K, Furstenberger G, Annan N, Kucher D, Pohl-Arnold A, Steinbauer B, Esposito I, Chiblak S, Friess H, Schirmacher P, et al. (2006). Preinvasive duct-derived neoplasms in pancreas of keratin 5–promoter cyclooxygenase-2 transgenic mice. *Gastroenterology* **130**, 2165–2178.
[32] Sandgren EP, Luetteke NC, Palmiter RD, Brinster RL, and Lee DC (1990). Overexpression of TGF alpha in transgenic mice: induction of epithelial hyperplasia, pancreatic metaplasia, and carcinoma of the breast. *Cell* **61**, 1121–1135.
[33] Hingorani SR, Petricoin EF, Maitra A, Rajapakse V, King C, Jacobetz MA, Ross S, Conrads TP, Veenstra TD, Hitt BA, et al. (2003). Preinvasive and invasive ductal pancreatic cancer and its early detection in the mouse. *Cancer Cell* **4**, 437–450.
[34] Schmied B, Liu G, Moyer MP, Hernberg IS, Sanger W, Batra S, and Pour PM (1999). Induction of adenocarcinoma from hamster pancreatic islet cells treated with *N*-nitrosobis(2-oxopropyl)amine *in vitro*. *Carcinogenesis* **20**, 317–324.
[35] Jimenez RE, Z'Graggen K, Hartwig W, Graeme-Cook F, Warshaw AL, and Fernandez-del Castillo C (1999). Immunohistochemical characterization of pancreatic tumors induced by dimethylbenzanthracene in rats. *Am J Pathol* **154**, 1223–1229.
[36] Ramirez A, Bravo A, Jorcano JL, and Vidal M (1994). Sequences 5′ of the bovine keratin 5 gene direct tissue- and cell-type–specific expression of a *lacZ* gene in the adult and during development. *Differentiation* **58**, 53–64.
[37] Thomson JM and Parrott WA (1998). pMECA: a cloning plasmid with 44 unique restriction sites that allows selection of recombinants based on colony size. *Biotechniques* **24**922–924, 926, 928.
[38] Hogan BCF and Lacy E (1986). *Manipulating the Mouse Embryo.* Cold Spring Harbor, NY: Cold Spring Harbor Laboratory Press.
[39] Gomez G, Lee HM, He Q, Englander EW, Uchida T, and Greeley GH Jr (2001). Acute pancreatitis signals activation of apoptosis-associated and survival genes in mice. *Exp Biol Med (Maywood)* **226**, 692–700.
[40] Gomez G, Englander EW, Wang G, and Greeley GH Jr (2004). Increased expression of hypoxia-inducible factor-1alpha, p48, and the Notch signaling cascade during acute pancreatitis in mice. *Pancreas* **28**, 58–64.
[41] Fischer SM, Lo HH, Gordon GB, Seibert K, Kelloff G, Lubet RA, and Conti CJ (1999). Chemopreventive activity of celecoxib, a specific cyclooxygenase-2 inhibitor, and indomethacin against ultraviolet light–induced skin carcinogenesis. *Mol Carcinog* **25**, 231–240.
[42] Jaffee EM, Schutte M, Gossett J, Morsberger LA, Adler AJ, Thomas M, Greten TF, Hruban RH, Yeo CJ, and Griffin CA (1998). Development and characterization of a cytokine-secreting pancreatic adenocarcinoma vaccine from primary tumors for use in clinical trials. *Cancer J Sci Am* **4**, 194–203.
[43] Bockman DE (1997). Morphology of the exocrine pancreas related to pancreatitis. *Microsc Res Tech* **37**, 509–519.
[44] Schussler MH, Skoudy A, Ramaekers F, and Real FX (1992). Intermediate filaments as differentiation markers of normal pancreas and pancreas cancer. *Am J Pathol* **140**, 559–568.
[45] Emberley ED, Murphy LC, and Watson PH (2004). S100 proteins and their influence on pro-survival pathways in cancer. *Biochem Cell Biol* **82**, 508–515.
[46] Moniaux N, Andrianifahanana M, Brand RE, and Batra SK (2004). Multiple roles of mucins in pancreatic cancer, a lethal and challenging malignancy. *Br J Cancer* **91**, 1633–1638.
[47] Crawford HC, Scoggins CR, Washington MK, Matrisian LM, and Leach SD (2002). Matrix metalloproteinase-7 is expressed by pancreatic cancer precursors and regulates acinar-to-ductal metaplasia in exocrine pancreas. *J Clin Invest* **109**, 1437–1444.
[48] Vu TH and Werb Z (2000). Matrix metalloproteinases: effectors of development and normal physiology. *Genes Dev* **14**, 2123–2133.
[49] Nakamura T, Kuwai T, Kim JS, Fan D, Kim SJ, and Fidler IJ (2007). Stromal metalloproteinase-9 is essential to angiogenesis and progressive growth of orthotopic human pancreatic cancer in parabiont nude mice. *Neoplasia* **9**, 979–986.
[50] Omary MB, Lugea A, Lowe AW, and Pandol SJ (2007). The pancreatic stellate cell: a star on the rise in pancreatic diseases. *J Clin Invest* **117**, 50–59.
[51] Apte MV, Park S, Phillips PA, Santucci N, Goldstein D, Kumar RK, Ramm GA, Buchler M, Friess H, McCarroll JA, et al. (2004). Desmoplastic reaction in pancreatic cancer: role of pancreatic stellate cells. *Pancreas* **29**, 179–187.
[52] Grippo PJ, Nowlin PS, Demeure MJ, Longnecker DS, and Sandgren EP (2003). Preinvasive pancreatic neoplasia of ductal phenotype induced by acinar cell targeting of mutant *Kras* in transgenic mice. *Cancer Res* **63**, 2016–2019.
[53] Jankowski JA, Harrison RF, Perry I, Balkwill F, and Tselepis C (2000). Barrett's metaplasia. *Lancet* **356**, 2079–2085.
[54] Tokoro T, Tezel E, Nagasaka T, Kaneko T, and Nakao A (2003). Differentiation of acinar cells into acinoductular cells in regenerating rat pancreas. *Pancreatology* **3**, 487–496.
[55] Sphyris N, Logsdon CD, and Harrison DJ (2005). Improved retention of zymogen granules in cultured murine pancreatic acinar cells and induction of acinar–ductal transdifferentiation *in vitro*. *Pancreas* **30**, 148–157.
[56] Liao JD, Adsay NV, Khannani F, Grignon D, Thakur A, and Sarkar FH (2007). Histological complexities of pancreatic lesions from transgenic mouse models are consistent with biological and morphological heterogeneity of human pancreatic cancer. *Histol Histopathol* **22**, 661–676.
[57] Strobel O, Dor Y, Alsina J, Stirman A, Lauwers G, Trainor A, Castillo CF, Warshaw AL, and Thayer SP (2007). *In vivo* lineage tracing defines the role of acinar-to-ductal transdifferentiation in inflammatory ductal metaplasia. *Gastroenterology* **133**, 1999–2009.
[58] Perides G, Tao X, West N, Sharma A, and Steer ML (2005). A mouse model of ethanol dependent pancreatic fibrosis. *Gut* **54**, 1461–1467.
[59] Schmid RM and Whitcomb DC (2006). Genetically defined models of chronic pancreatitis. *Gastroenterology* **131**, 2012–2015.

[60] Saluja AK, Lerch MM, Phillips PA, and Dudeja V (2007). Why does pancreatic overstimulation cause pancreatitis? *Annu Rev Physiol* **69**, 249–269.

[61] Al-Aynati MM, Radulovich N, Riddell RH, and Tsao MS (2004). Epithelial-cadherin and beta-catenin expression changes in pancreatic intraepithelial neoplasia. *Clin Cancer Res* **10**, 1235–1240.

[62] Zeng G, Germinaro M, Micsenyi A, Monga NK, Bell A, Sood A, Malhotra V, Sood N, Midda V, Monga DK, et al. (2006). Aberrant Wnt/beta-catenin signaling in pancreatic adenocarcinoma. *Neoplasia* **8**, 279–289.

[63] Herold K, Moser B, Chen Y, Zeng S, Yan SF, Ramasamy R, Emond J, Clynes R, and Schmidt AM (2007). Receptor for advanced glycation end products (RAGE) in a dash to the rescue: inflammatory signals gone awry in the primal response to stress. *J Leukoc Biol* **82**, 204–212.

[64] Lohr M, Kloppel G, Maisonneuve P, Lowenfels AB, and Luttges J (2005). Frequency of K-*ras* mutations in pancreatic intraductal neoplasias associated with pancreatic ductal adenocarcinoma and chronic pancreatitis: a meta-analysis. *Neoplasia* **7**, 17–23.

[65] Smakman N, Kranenburg O, Vogten JM, Bloemendaal AL, van Diest P, and Borel Rinkes IH (2005). Cyclooxygenase-2 is a target of KRASD12, which facilitates the outgrowth of murine C26 colorectal liver metastases. *Clin Cancer Res* **11**, 41–48.

[66] Jhappan C, Stahle C, Harkins RN, Fausto N, Smith GH, and Merlino GT (1990). TGF alpha overexpression in transgenic mice induces liver neoplasia and abnormal development of the mammary gland and pancreas. *Cell* **61**, 1137–1146.

[67] Lewis BC, Klimstra DS, and Varmus HE (2003). The c-*myc* and *PyMT* oncogenes induce different tumor types in a somatic mouse model for pancreatic cancer. *Genes Dev* **17**, 3127–3138.

[68] Cano DA, Sekine S, and Hebrok M (2006). Primary cilia deletion in pancreatic epithelial cells results in cyst formation and pancreatitis. *Gastroenterology* **131**, 1856–1869.

[69] Shintaku M, Arimoto A, and Sakita N (2005). Serous cystadenocarcinoma of the pancreas. *Pathol Int* **55**, 436–439.

[70] Strobel O, Z'Graggen K, Schmitz-Winnenthal FH, Friess H, Kappeler A, Zimmermann A, Uhl W, and Buchler MW (2003). Risk of malignancy in serous cystic neoplasms of the pancreas. *Digestion* **68**, 24–33.

[71] Kosmahl M, Pauser U, Anlauf M, and Kloppel G (2005). Pancreatic ductal adenocarcinomas with cystic features: neither rare nor uniform. *Mod Pathol* **18**, 1157–1164.

[72] Tada M, Kawabe T, Arizumi M, Togawa O, Matsubara S, Yamamoto N, Nakai Y, Sasahira N, Hirano K, Tsujino T, et al. (2006). Pancreatic cancer in patients with pancreatic cystic lesions: a prospective study in 197 patients. *Clin Gastroenterol Hepatol* **4**, 1265–1270.

[73] Gomez D, Rahman SH, Won LF, Verbeke CS, McMahon MJ, and Menon KV (2006). Characterization of malignant pancreatic cystic lesions in the background of chronic pancreatitis. *JOP* **7**, 465–472.

[74] Volkan Adsay N (2007). Cystic lesions of the pancreas. *Mod Pathol* **20** (Suppl 1), S71–S93.

[75] Kloppel G (2007). Chronic pancreatitis, pseudotumors and other tumor-like lesions. *Mod Pathol* **20** (Suppl 1), S113–S131.

[76] Raut CP, Nawrocki S, Lashinger LM, Davis DW, Khanbolooki S, Xiong H, Ellis LM, and McConkey DJ (2004). Celecoxib inhibits angiogenesis by inducing endothelial cell apoptosis in human pancreatic tumor xenografts. *Cancer Biol Ther* **3**, 1217–1224.

[77] Wei D, Wang L, He Y, Xiong HQ, Abbruzzese JL, and Xie K (2004). Celecoxib inhibits vascular endothelial growth factor expression in and reduces angiogenesis and metastasis of human pancreatic cancer via suppression of Sp1 transcription factor activity. *Cancer Res* **64**, 2030–2038.

[78] Ali S, El-Rayes BF, Sarkar FH, and Philip PA (2005). Simultaneous targeting of the epidermal growth factor receptor and cyclooxygenase-2 pathways for pancreatic cancer therapy. *Mol Cancer Ther* **4**, 1943–1951.

[79] Jimeno A, Amador ML, Kulesza P, Wang X, Rubio-Viqueira B, Zhang X, Chan A, Wheelhouse J, Kuramochi H, Tanaka K, et al. (2006). Assessment of celecoxib pharmacodynamics in pancreatic cancer. *Mol Cancer Ther* **5**, 3240–3247.

[80] El-Rayes BF, Zalupski MM, Shields AF, Ferris AM, Vaishampayan U, Heilbrun LK, Venkatramanamoorthy R, Adsay V, and Philip PA (2005). A phase II study of celecoxib, gemcitabine, and cisplatin in advanced pancreatic cancer. *Invest New Drugs* **23**, 583–590.

[81] Xiong HQ, Plunkett W, Wolff R, Du M, Lenzi R, and Abbruzzese JL (2005). A pharmacological study of celecoxib and gemcitabine in patients with advanced pancreatic cancer. *Cancer Chemother Pharmacol* **55**, 559–564.

[82] Cascinu S, Scartozzi M, Carbonari G, Pierantoni C, Verdecchia L, Mariani C, Squadroni M, Antognoli S, Silva RR, Giampieri R, et al. (2007). COX-2 and NF-κB overexpression is common in pancreatic cancer but does not predict for COX-2 inhibitors activity in combination with gemcitabine and oxaliplatin. *Am J Clin Oncol* **30**, 526–530.

[83] Schuller HM, Kabalka G, Smith G, Mereddy A, Akula M, and Cekanova M (2006). Detection of overexpressed COX-2 in precancerous lesions of hamster pancreas and lungs by molecular imaging: implications for early diagnosis and prevention. *ChemMedChem* **1**, 603–610.

[84] Funahashi H, Satake M, Dawson D, Huynh NA, Reber HA, Hines OJ, and Eibl G (2007). Delayed progression of pancreatic intraepithelial neoplasia in a conditional Kras(G12D) mouse model by a selective cyclooxygenase-2 inhibitor. *Cancer Res* **67**, 7068–7071.